Journal of Applied Geophysics 217 (2023) 105186

Contents lists available at ScienceDirect

Journal of Applied Geophysics

journal homepage: www.elsevier.com/locate/jappgeo

The drone-borne magnetic survey as the optimal strategy for high-resolution investigations in presence of extremely rough terrains: The case study of the Taverna San Felice quarry dike

Filippo Accomando [a,*], Antonello Bonfante [b], Maurizio Buonanno [b], Jacopo Natale [c], Stefano Vitale [a], Giovanni Florio [a]

[a] Department of Earth, Environmental and Resources Sciences, University of Naples "Federico II", Naples 80126, Italy
[b] ISAFOM, Consiglio Nazionale Delle Ricerche (CNR), Portici (NA), 80055 Portici, Italy
[c] Department of Earth and Geoenvironmental Sciences, University of Bari Aldo Moro, Italy

ARTICLE INFO

Keywords:
Magnetic surveys
Unmanned aerial vehicle
Spectral analysis
Magnetic noise
Potential field

ABSTRACT

In the Taverna San Felice limestone active quarry (Italy) excavation has progressively exposed a magmatic dike embedded in a calcareous succession. The dike outcrops are scattered among the high vertical steps of the quarry, whereas outside the excavated area the steep mountain slope covered by a dense bush vegetation make direct inspection and geological mapping a challenging task. To map the areal extension of the dike and to define its direction and its relationship with tectonic lines over an area larger than the quarry, a magnetic survey was performed. Given the above-mentioned extremely rugged terrain, a UAV-based magnetic survey was the preferred acquisition strategy. Data were acquired by rigidly fixing the magnetometer to the UAV landing sled, using a sensor with a very high-frequency (1000 Hz) acquisition rate. The acquisition strategy and some simple processing steps resulted in a detailed drone-borne total field anomaly map. This dataset allowed for a mapping of the dike outside the quarry area and the identification of a vent fed by the dike. The 2D forward modelling of the magnetic data was constrained by a field estimation of the intensity of the total magnetization and by the depth to the dike's top, in places where it is outcropping.

1. Introduction

The magnetic method is one of the oldest and most widely used near-surface geophysics exploration techniques. It allows a rapid, cheap, reliable, and non-invasive measurement of the Earth's magnetic field. Magnetic surveys have application in geological, archaeological, and engineering problems, from small to large scales of investigation. Recent advances in geophysical sensors and the development of unmanned aerial vehicles (UAV), commonly known as drones, allowed miniaturized and lightweight magnetometers to be integrated with UAV platforms. The use of drones reduces costs, time, and risks compared to other acquisition techniques while allowing the realization of surveys with a very high resolution and uniform aerial coverage. These advantages make UAV magnetic surveys a practical and often preferable alternative to the standard ground and airborne surveys.

However, in specific and difficult ground conditions, the UAV magnetic survey could be complex, but at the same time, the only alternative for data acquisition. These ground conditions include the presence of dense vegetation, cultivated areas, swamps, glaciers, lakes, foreshore areas or steep mountain slopes. In these cases, standard approaches to ground surveys may not be feasible, and high-altitude airborne prospections may not provide the requested spatial resolution. In literature, several authors have demonstrated the efficacy of UAV aeromagnetic data collection and proposed different flight configurations, highlighting that the main problem related to UAV magnetic surveys is the magnetic and electromagnetic disturbance due to the UAV platforms (Malehmir et al., 2017; Parvar et al., 2018; Walter et al., 2020; Nikulin et al., 2020; De Smet et al., 2021; Parshin et al., 2018; Walter et al., 2019a; Walter et al., 2019b; Walter et al., 2021; Li et al., 2018; Phelps et al., 2022). The proposed solutions consist in suspending the magnetometer sensors 2–5 m away from the drone motors or by attempting some post-acquisition filtering of the data (Mu et al., 2020).

* Corresponding author.
E-mail addresses: filippo.accomando@unina.it (F. Accomando), maurizio.buonanno@cnr.it (M. Buonanno), jacopo.natale@uniba.it (J. Natale), stefano.vitale@unina.it (S. Vitale), gflorio@unina.it (G. Florio).

https://doi.org/10.1016/j.jappgeo.2023.105186
Received 27 April 2023; Received in revised form 26 July 2023; Accepted 10 September 2023
Available online 12 September 2023

However, hanging the magnetometer sensor to the drone with long ropes can create unwanted periodic variations in the acquired magnetic data, generated by the oscillations of the magnetometer sensor. Moreover, the suspended weight may cause flight instabilities and can increase the flight-related hazard, for instance in presence of vegetation near the programmed flight altitude or in case of non-optimal weather conditions. In fact, when it is necessary to increase flight security and stability, at least in the case of surveys over intense magnetic anomalies, a practical solution for carrying the magnetometer may be to rigidly attach it to the drone's landing gear (at only about 0.50 m from the engines; Accomando et al., 2021). Other authors propose safer solutions using shorter suspension distances (about 1 m; Veloski et al., 2018; Kaub et al., 2021) or avoiding suspending the magnetometer by mounting the magnetometer at the end of a fixed large arm (Cunningham, 2018; Tuck et al., 2019).

In this study, we present the results of a drone-borne magnetic survey aimed at mapping an igneous dike intruded in sedimentary rocks, which was exposed by excavation activities in an active quarry. We chose to attach the magnetometer to the landing gear of a drone as the best option to overcome the limitations to ground data acquisition posed by the complex terrain geometry, the steepness of the slope, the presence of bush vegetation, and ongoing extraction activities.

In the following, the geologic setting will be briefly described, then the magnetic survey will be presented with details, along with the processing and the modelling of the data and the final geologic conclusions.

2. Geological setting

The study area (WGS84, 41.364338° N, 14.036985° E) is an active quarry for limestone extraction, at Taverna San Felice, near the town of Presenzano (Campania Region, southern Italy), on the southwestern slope of the Mt. Cesima ridge, northeast of Roccamonfina volcano (Fig. 1a). This part of the southern Apennines is characterized by a Pleistocene structural depression (Garigliano Graben, Fig. 1a) hosting the Roccamonfina volcano, whose activity ranged between 630 and 50 ka (e.g., Conticelli et al., 2009), mainly emplacing lavas and scoriae from scattered vents, and ignimbrites from the summit area (e.g., De Rita and Giordano, 1996).

Since the late 1980s, excavation activities in the Taverna San Felice quarry have progressively exposed a magmatic dike embedded in a dominant calcareous succession formed by well-bedded Lower Cretaceous limestones (Calcari a Requenie Fm.), covered by Upper Cretaceous-Paleocene breccias (Calcari Cristallini Fm.), and Lower Pleistocene breccias (Vitale and Ciarcia, 2018). At the base of the quarry, the magmatic dike is broadly oriented *E*-W and moderately dipping northward, switching to sub-vertical and NE-SW oriented moving upward (Fig. 1b, c; Natale et al., 2023). The dike is composed of a main sheet, over 250 m long and with thickness varying in the range of 5–25 m and several minor apophysis, a few meters long. The contact between the dike and the host rock is sharp and regular at the base, while it is more irregular towards the top of the quarry (Natale et al., 2023). The dike fed a fissure eruption that emplaced up to 10–15 m thick

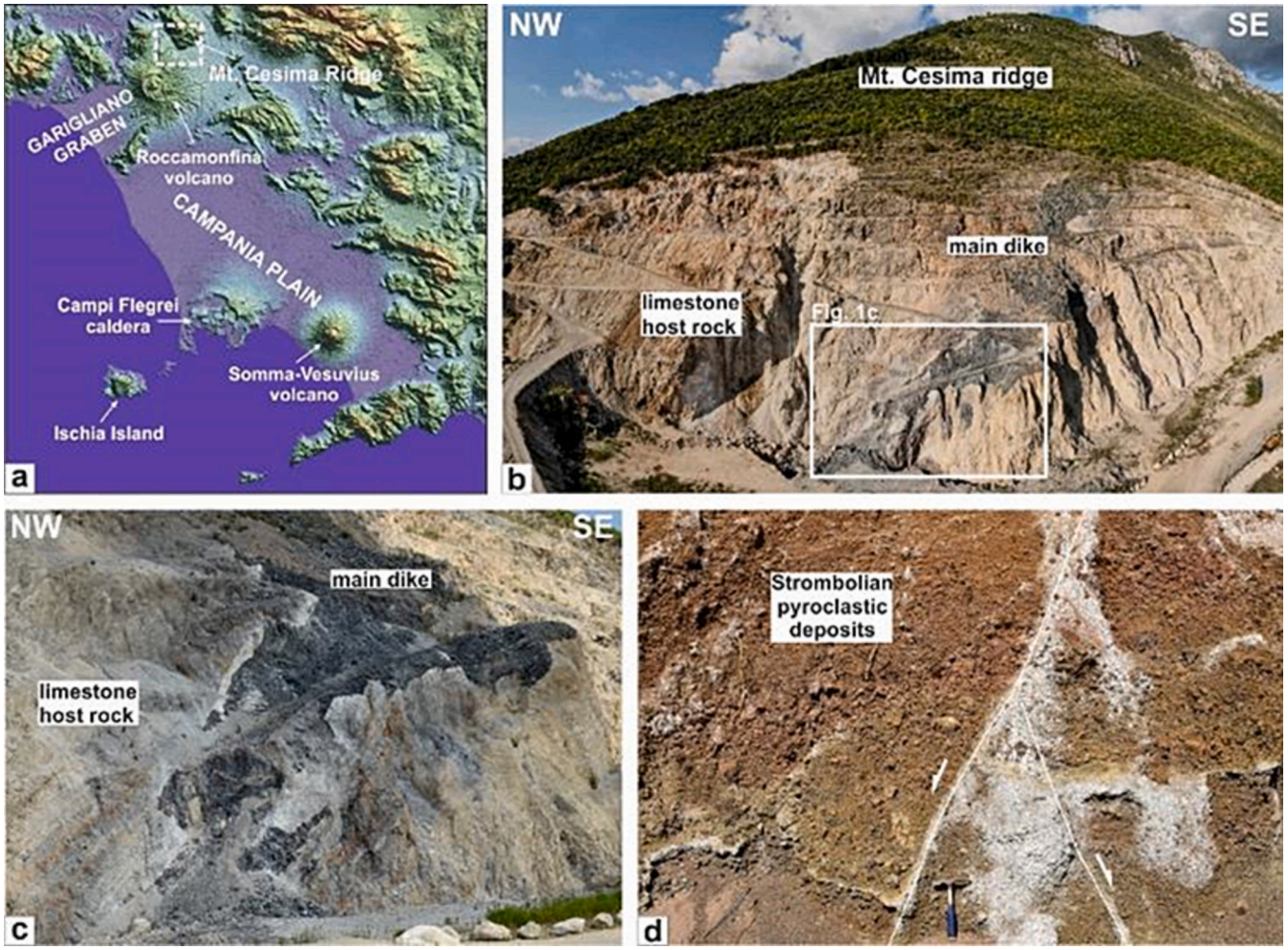

Fig. 1. (a) Location of the study area with respect to the main volcanic centres of Campania Plain (southern Italy). (b) Wide-angle UAV picture of the Taverna San Felice quarry excavation front. Location of Fig. 1c is marked by the white box. (c) Detail of the contact between the magmatic dike and the carbonatic host rock at the base of the quarry excavation front. (d) Example of the Strombolian pyroclastic succession exposed in the upper part of the quarry.

Strombolian deposits, which mainly crops out in the upper part of the quarry and reworked at the base of the slope. These deposits overlay a series of altered pyroclastic deposits ascribed to Roccamonfina volcano (Natale et al., 2023; Fig. 1d). The dike and its tephra pertain to tephrites-phonotephrites compositions (Natale et al., 2023), overlapping with the compositions reported in Di Girolamo et al. (1991). In the upper part of the quarry, welded spatter ramparts occur, representing the preserved record of the vent system (Natale et al., 2023). The dike outcrops are scattered among the several 5 m high vertical steps of the quarry, whereas outside the excavated area the steep slope covered by a dense bush vegetation make direct inspection and geological mapping a challenging task. To better understand the aerial extension of the dike and the related volcanic products and to define its direction and its relationship with tectonic lines over an area larger than the quarry, a magnetic survey was planned. Given the above-mentioned ground conditions, a UAV-based magnetic survey was the preferred acquisition strategy.

3. Measurements and survey design

The drone-borne magnetic survey was conducted during April and May 2022.

The UAV used for this acquisition is a DJI Matrice 600 Pro hexacopter (hereafter M600P), which can fly for 32 min without payload and a maximum of 22 min with a payload of 2 kg according to atmospheric conditions (e.g., wind speed).

UAV magnetic data were collected using the Geometrics Micro-Fabricated Atomic Magnetometer (MFAM) in the "Development kit" version (hereafter MFAM-DK), which includes a laser-pumped atomic magnetometer with two cesium alkali-vapor sensors and a development board with an onboard GPS module. The high sampling rate of 1000 Hz allows obtaining an unaliased measurement of 50 Hz fields relative to power lines and the correct identification of the high-frequency magnetic noise caused by the propellers (Walter et al., 2021). This specification, in addition to the small weight (about 1 kg) and the high sensitivity, make this magnetometer ideal to be integrated in a UAV system.

The MFAM-DK was housed inside a light, aerodynamic and nonmagnetic custom bird, made of polystyrene, having a thin and rigid base (a Nomex honeycomb sandwich panel). The total payload weight was <2.0 kg (Fig. 2a).

One of the main choices affecting the data quality and the operativity of the UAV system regards the way the magnetometer is attached to the drone. To overcome the difficulty of flying along irregular and steep terrain (slope > 60%; Fig. 2c), and to improve flight safety, we chose to attach the magnetometer to the drone's landing gear, at only 0.50 m from the engines (Fig. 2b). Moreover, this choice prevents the generation of noise in the data due to magnetometer swinging when it is attached to the UAV with long ropes.

In such configuration, the data are contaminated by an intense high-frequency noise generated by static and time-varying magnetic fields. However, these effects are confined to the high-frequency part of the spectrum with a major peak at 50 Hz. Thanks to the very high sampling step of the MFAM magnetometer they can be correctly sampled, easily identified in the spectrum, and removed with a low pass filtering. The high amplitude of this noise (more of 20 nT in this survey) implies that such a configuration could be used only when strong magnetic anomalies are expected (Accomando et al., 2021). This is the case of a shallow magmatic intrusion surveyed at a few meters' altitude, where simple forward models show total field anomalies with an amplitude few

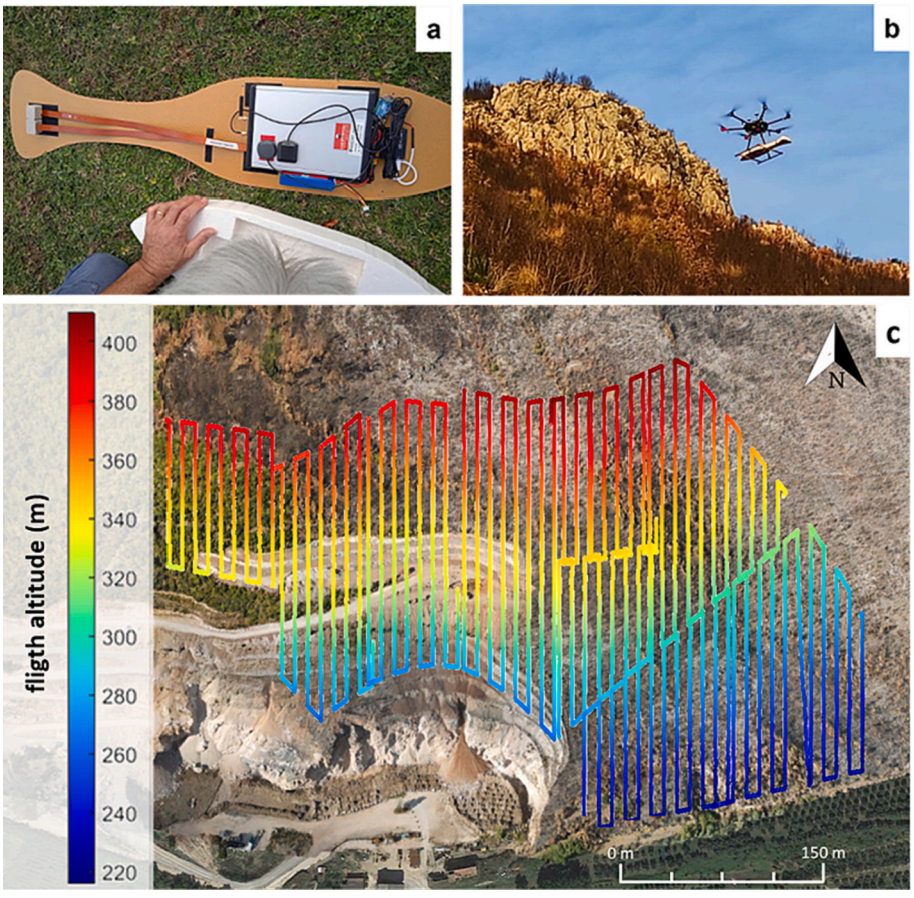

Fig. 2. (a) Arrangement of the Geometrics MFAM "Development kit" magnetometer inside the prototype bird; (b) Field photograph showing the flight configuration with the magnetometer fixed to the platform landing sled, 0.5 m below the UAV; (c) Flight paths and altitude variation along the surveyed lines.

hundreds of nT.

Nine individual flight surveys were needed to cover the study area at an elevation of 20 m AGL (above ground level), and 81 parallel survey lines were flown with a 10 m horizontal line separation. To ensure flight safety and constant height above terrain, flight missions were planned using a high-resolution DSM (1 m × 1 m) generated with photogrammetric data surveyed just before the magnetic acquisitions.

Surveys profiles were oriented along a direction approximately North–South to maximize the magnetometer performance and avoid falling into the sensors dead zone. To prevent the magnetic heading error, the flights were performed avoiding the 180° turn at the end of each survey line, as suggested by (Accomando et al., 2021). Overall, the duration of each flight was approximately 15 min long and a total of over 16 km in a linear distance of magnetic data were acquired. The geomagnetic field in this area had a declination of 4° and an inclination of 57°.

With MFAM-DK operating at 1000 Hz and with a flight speed of about 2 m/s, the sampling step of the magnetic data along the survey lines was as small as about 2 mm. Since the built-in GPS receiver of the MFAM-DK did not produce satisfactory results, the positional data recorded by the UAV's GPS were used instead (declared horizontal accuracy ±1.5 m). Magnetic data were synchronized with UAV positional data by means of the GPS time simultaneously recorded by both the MFAM-DK and M600P GPS receivers. As the magnetic sensor is rigidly fixed to the drone landing gear, as explained later, there is no horizontal offset between the magnetometer and the UAV so that we geo-localized the magnetic data using directly the coordinates recorded by the internal GNSS receiver of the drone.

4. Results

4.1. Total field magnetic anomalies

The data analysis included the removal of the magnetic data recorded during the drone turns at the end of each profile, as they may have a reduced accuracy. As the surveyed area has a limited extension, the International Geomagnetic Reference Field (IGRF) was approximated by a single constant value (46,548.5 nT) that was subtracted to all the datasets. The diurnal variation of the magnetic field, monitored by a GEM Overhauser magnetometer at a station near the survey area, was negligible in the time span of a single flight, so no temporal correction was applied to the nine datasets, also considering the strong amplitude of the measured anomalies. A constant level adjustment of a few nT among the data collected in the various flights, done in the same day or in different days, was instead necessary. The resulting unfiltered Total-Field Anomaly (TFA), as displayed in the example profile of Fig. 3, shows a high-frequency noise with a peak-to-peak amplitude of about 25 nT that characterizes the signal during all the flight duration. This disturbance is associated to the magnetic and electromagnetic interference fields generated by the UAV platform, and its high amplitude is due to the small distance between the drone engines and magnetic sensors (0.5 m).

Spectral analysis in the wavelet time-scale domain guided us in exploring the variation of the frequency content of the data through time, distinguishing the noise and signal components of the data. Here, through the continuous wavelet transform (CWT) we obtained a scalogram of the datasets in the time domain using a "Morse wavelet" and we present the modulus of the complex set of CWT coefficient for the drone-borne datasets (Fig. 4a). The sum of the scalogram at each frequency (Fig. 4b) summarizes the spectral content of the data. The prominent peak around 50 Hz can be interpreted by the presence of a significant platform-induced magnetic and electromagnetic interference sensed by the magnetometer and to, a lesser extent, also the electrical power lines present in the area.

By this analysis, we could highlight the ability of MFAM-DK to correctly sample high-frequency magnetic noise as well as other peaks at smaller frequencies, not associable with geological sources. In fact, to estimate the frequency band associated with the target signal, we can evaluate the ratio of the UAV speed and the horizontal anomaly extent (representing a half-wavelength of the signal) multiplied by two (Walter et al., 2021). In our case, the data analysis along each flight profile shows that the geological sources should have an anomaly half-wavelength of about 40–80 m (Fig. 3a). Considering the UAV speed of 2 m/s, we estimate a target signal frequency band between 0.0125 Hz and 0.025 Hz. Thus, we designed a Hanning-window low-pass filter in the time-domain with a cut-off frequency of 1 Hz, which removes the noise and preserves the lower frequency signal associated to the geological sources.

The filtered data collected along the 81 profiles were interpolated on a 2.5 m × 2.5 m grid to have a map of the magnetic anomalies in the

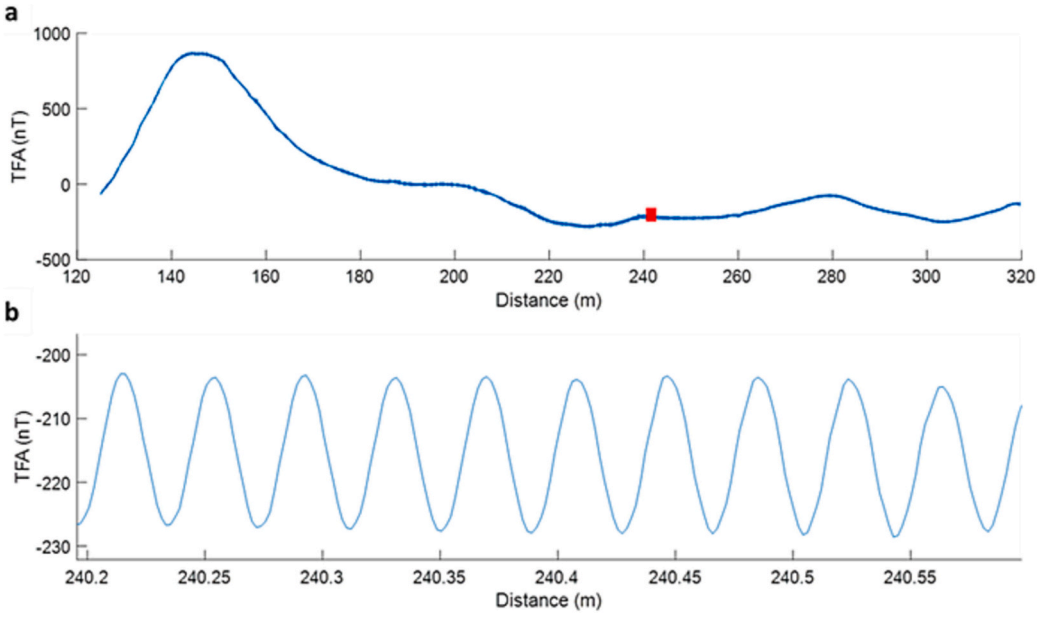

Fig. 3. Unfiltered Total-Field Anomaly (TFA) acquired along the profile n. 31; b) the unfiltered data enclosed in the red rectangle in Fig. 3a. (For interpretation of the references to colour in this figure legend, the reader is referred to the web version of this article.)

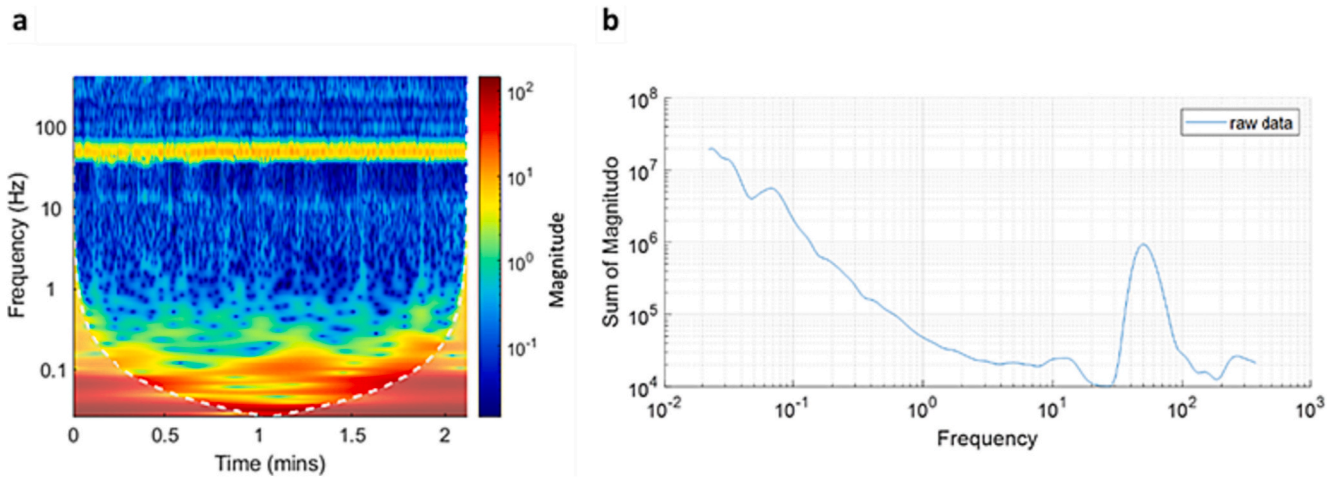

Fig. 4. Continuous wavelet transform (CWT) analysis of the magnetic dataset. a) Time-domain scalogram of the unfiltered TFA acquired along the profile n. 31, computed using a "Morse" wavelet; b) Sum of the scalogram magnitude at each frequency.

area. Fig. 5 shows the total field magnetic anomalies detected in the study area, presenting a maximum amplitude variation of about 1600 nT, ranging from about −400 to 1200 nT. The magnetic effect of the dike can be identified as a linear magnetic high trending WSW-ENE, from the quarry area, where it is outcropping, to the mountain slope. There, the magnetic high assumes a nearly elliptical shape, slightly elongated in a NW-SE direction. The variation of the amplitude of the linear anomaly can be easily correlated with its depth to the top, with the highest values related to the outcropping part. South of the circular feature it can be noticed the presence of an isolated smaller anomaly. It is interesting to notice how these very intense main anomalies identify a well delimited area with the magnetic field decreasing abruptly outside it. This evidence can be ascribed to the presence of very shallow, or even outcropping, magnetized rocks. Other minor anomalies north of the linear anomaly are instead unrelated to the volcanic products and being generated by trucks and excavators present there during the survey.

4.2. Forward modelling

A subsurface model can provide important information for geological interpretation. For example, it can suggest a probable propagation mechanism of the intrusion, and its thicknesses, providing a useful information for the reconstruction of the stress field at the time of the intrusion or for studying the influence of pre-existing faults that could have influenced its direction. Therefore, we performed a 2.5D forward modelling along three different sections (Fig. 7a) to reconstruct a model, giving some geological insights. The modelling was performed by commercial software based on the method described by Talwani and Heirtzler (1964) and Won and Bevis (1987). As the magnetic models suffer nonuniqueness, they must be constrained by independent information. We performed a field experiment concerning the estimate of the intensity of the total magnetization (induced plus remanent) of the dike rocks, according to the method outlined by Breiner (1973). This method is based on the identification of the maximum value of the total field recorded by a total field magnetometer while a rock sample is rotated at a certain distance from the sensor along the local direction of the magnetic field. The method assumes that the rock sample can be considered as a dipolar source. In our case, we used two rock samples having a roughly spherical shape. The volume of the samples was 331 cm^3 (sample #1) and 1495 cm^3 (sample #2). The test was repeated three times for each sample and the maximum total field value recorded was retained and used for the magnetization estimate (Fig. 6). Although the method is expected to provide only a rough estimate of the total magnetization, in our case the results were satisfying in that the estimated value is very similar for the two samples (16.5 A/m and 16.1 A/m). Thus, we considered the estimated values as representative of the total magnetization, and the average value of 16.3 A/m was used as a constraint for our forward modelling.

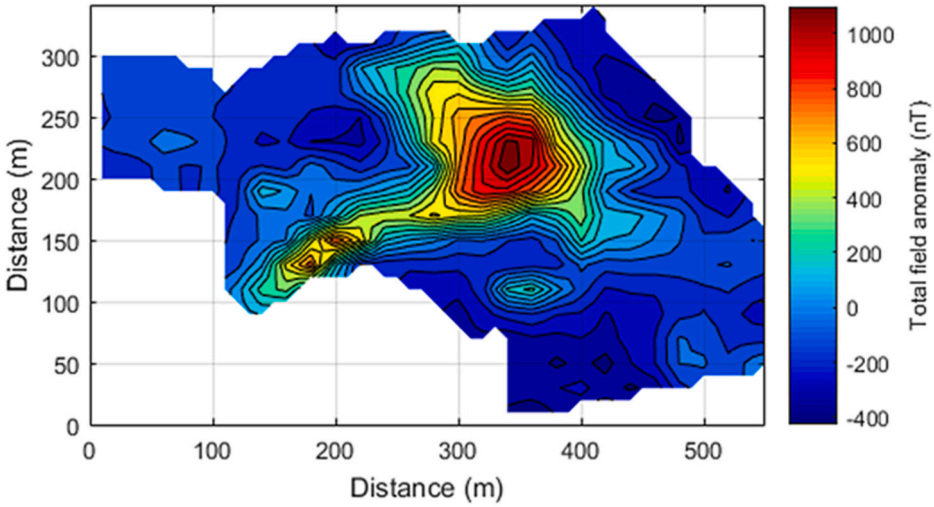

Fig. 5. Total field anomaly map obtained from filtered data.

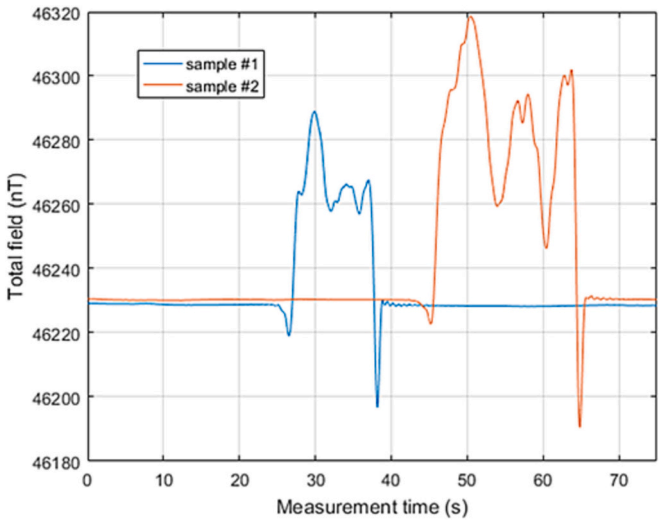

Fig. 6. Total magnetization estimations by the Breiner (1973) method. The two curves represent the total field variation caused by the presence of rotating igneous rock samples. The flat parts of the curves are relative to the background magnetic field in the absence of the rock samples. The rotation of the samples may cause the alignment of the induced and remanent magnetization vectors, resulting in the maximum total field value recorded. According to the Breiner (1973) method, the maximum value is combined with the sample volume and the distance separating the rock sample and the magnetometer sensor to estimate the total magnetization.

The first profile (section A-A', in Fig. 7a) orthogonally crosses the part of the dike outcropping along the quarry wall. Thus, in this case, we could model the source of the magnetic field using two solid constraints, namely the depth to source's top (0 m) and its magnetization (16.3 A/m). We could fit the total field anomaly satisfactorily by assuming a dike thickness of 8.5 m and if the dike steeply dips northward with an angle of about 80°. The observed data show northwest of the dike anomaly another magnetic anomaly related to the presence of trucks and excavators during the survey, which was not considered in the modelling. To account for the limited extension of the dike in the W direction, the 2.5D model has a length of 50 m in the westerly strike direction. The misfit between the observed and predicted data may be evaluated by the relative error, defined as:

$$\frac{\|obs - pred\|}{\|obs\|} \text{ x } 100 \quad (1)$$

where *obs* stands for the observed total field anomaly, *pred* stands for the magnetic data predicted by the model and $\|\bullet\|$ stands for the L2 norm. In the case of profile A-A', the relative error was 6.35% when considering only the South-Eastern part of the profile, relative to the dike anomaly.

The second profile (B-B′ in Fig. 7a) crosses the dike anomaly in an area, east of the previous profile, where it is not outcropping. In this case, we constrained the model using the estimated total magnetization, and the same thickness and dip as estimated in the modelling of the A-A' profile, and we could constrain the depth to the top of the buried body, which resulted to be about 7–8 m (Fig. 7c). This profile crosses the dike anomaly at its approximate center, so that a 2D model is reasonable in this case. To the north of the dike anomaly, another anomaly, less intense, can be noticed. The analysis of the total field anomaly map (Fig. 7a) allows to easily associate it to the main circular anomaly further east. However, we tried to model only the anomaly clearly related to the dike, neglecting this feature as well as the South-Eastern tail of the main anomaly along this profile, clearly influenced by the effects of other sources. The resulting model predicts a field that has a relative error of 6.68% (the error was computed only in the central part of the profile, including only the main anomaly).

The third profile (C-C′ in Fig. 7a) crosses the main and most intense magnetic anomaly. Geologic field work allowed to relate it to the presence of Strombolian pyroclastic succession and welded spatter ramparts, probably associated to the eruption fed by the dike (Natale et al., 2023). Also in this case, we use the dike magnetization, thickness and dip as a-priori information. We built a model where the dike is present at a depth of about 8 m while, at shallower depth and outcropping, a layer of welded spatter and pyroclastic deposits (having a maximum thickness of 10–15 m) is present. The magnetization of the volcanic products is considered to be the same of the main magmatic body. In this case the modelled sources in the direction of strike extend to 75 m. To the South of the main anomaly, another magnetic high is clearly visible. It is modelled with the presence of shallow to outcropping volcanic material, but it may be equally well justified by a deeper source, perhaps a branch of the main dike. We did not try to fit the magnetic profile south of this last anomaly, probably generated by other sources not crossed by the profile. The relative error for the data predicted by this model is 4.23% (the error was computed excluding the southern tail of the anomaly profile).

Finally, we tested the modelling sensitivity to the dike inclination. Thus, we varied the dip of the model dike along the profile B-B′ shown in Fig. 7c by ±10°, leaving the other model parameters unchanged. The resulting models are presented in Fig. 8. It is clear that the 10° variation in dip produces strong variations in the predicted field, with large relative errors of the field produced by these alternative models (44% for a vertical dike, 52% for a dip of 70°). Thus, the estimated dike inclination of 80°, obtained from the model along the A-A' profile, should be considered as a rather reliable indication about the true dike dip angle.

5. Discussion

We mapped an igneous dike partially emerging along a quarry wall and could follow its trace and the related volcanic products on a steep mountain slope. The use of the drone allowed a high-resolution, safe and rapid investigation despite the dangerous excavation areas of the quarry and the dense vegetation surrounding it. The MFAM-DK magnetometer was fixed directly to the drone landing sled. This solution increased the stability and security of the flight and is practicable from the signal-to-noise ratio point of view, considering the intense magnetic anomalies due to the strong magnetization contrast between volcanic and sedimentary rocks. However, flying with the sensor very close to the UAV engines amplifies the noise due to the magnetic and electromagnetic interference having a peak frequency at about 50 Hz, as shown in the scalogram of Fig. 4. Walter et al. (2021) showed as the slightly nonsymmetric magnetic field of all permanent magnet pairs presents in the drone motors produces a magnetic interference signal equal to the mechanical rotation frequency of the rotor (which is around 50 Hz). This strong signal sums up to the power grid signal at around the same 50 Hz frequency. The use of a high-frequency sampling magnetometer such as the MFAM-DK (1000 Hz) allowed us to correctly sample and identify the intense high-frequency interference around 50 Hz. This signal can be removed effectively with a simply designed low-pass filter. However, in the case of magnetometers with lower sampling rates the magnetic and electromagnetic noise would be under sampled and aliased in the acquired magnetic data. This aliased signal may require additional filtering that may degrade the data quality. Moreover, Walter et al. (2021) shows that there might be other interferences at frequencies even higher than the MFAM-DK Nyquist frequency (500 Hz), although with amplitude from 1/10 to 1/80 of that of the 50 Hz signal, so that the importance of these potentially aliased components is probably negligible.

For navigation, we decided to use the drone GNSS receiver without equipping the platform with RTK system. Especially in mountain areas, the probability of losing the radio link with the base station during a flight is high. In these cases, corrections would not be transmitted to the GNSS drone system, and this would result in a decrease in accuracy from

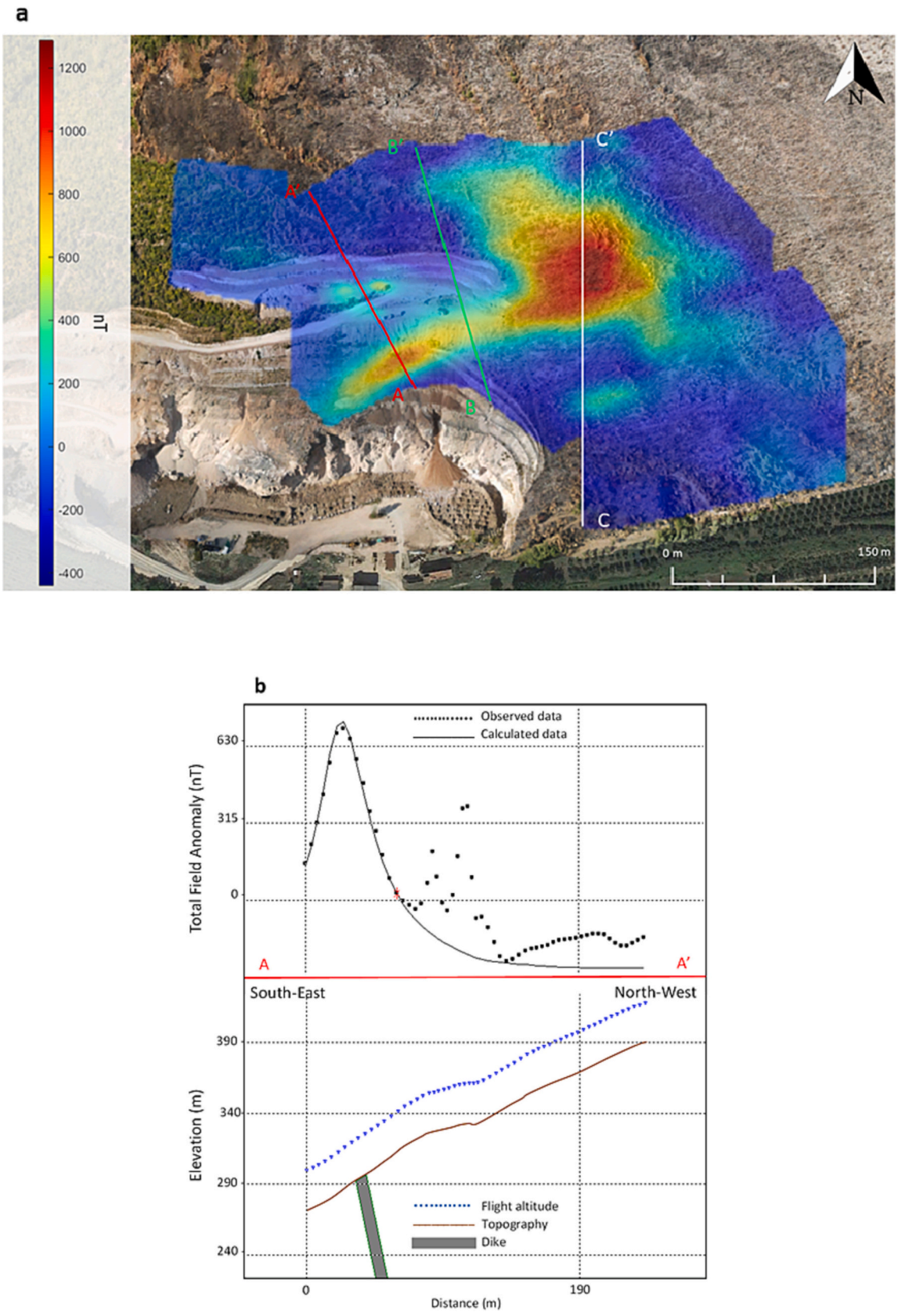

Fig. 7. Forward modelling. (a) Total field magnetic anomalies superimposed on a satellite image of the survey area. The lines identify the positions of the three modelled profiles. (b) Source modelling along the profile A-A'. (c) Source modelling along the profile B-B′. (d) Source modelling along the profile C-C′.

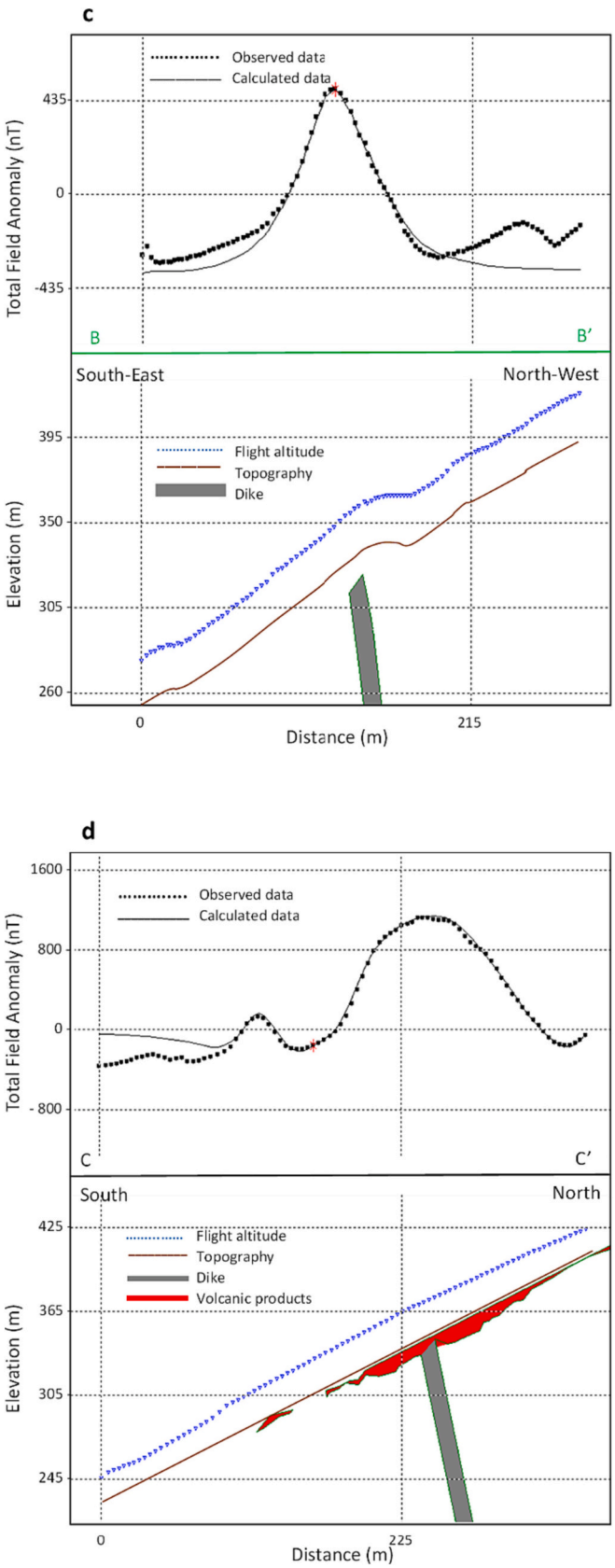

Fig. 7. (*continued*).

3 to a few dozen of meters. The largest error will be in the flight elevation, and this could be very dangerous in the case of surveys over terrain with dense and high vegetation for the entire flight system, with the risk of losing the instrumentation. Instead, before the magnetic acquisition, a photogrammetry survey was conducted, and a Digital Surface Model (DSM) of the terrain was obtained. This terrain model was

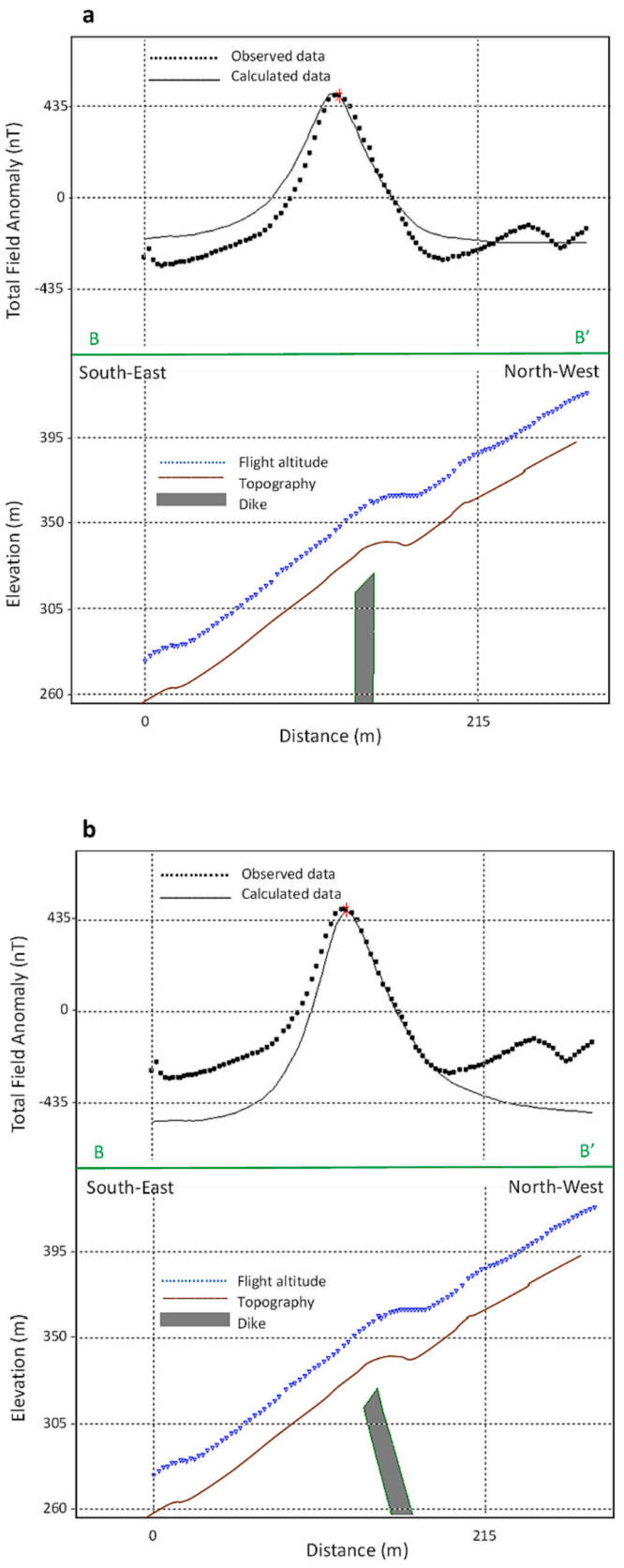

Fig. 8. Test of the modelling sensitivity to the dike inclination along the profile B-B′. (a) Source modelling increasing the dike inclination of 10° (the dike is vertical); (b) Source modelling de-creasing the dike inclination of 10° (the dike inclination is 70°).

used to plan the flight route and to choose a safe acquisition elevation.

These technical features of the UAV survey allow to acquire high-quality data. The strong high frequency noise due to the small distance from the platform, was characterized by a spectral analysis and removed without affecting the geologic signal of interest, which occurs at a much lower frequency band.

The filtered data showed the presence of an intense linear magnetic anomaly. This anomaly, very well correlated to the outcropping part of the dike, suggests a NE-SW orientation of the main intrusive body in the uppermost part of the quarry. At about 150 m from the quarry wall, an intense elliptical magnetic anomaly, with its major axis perpendicular to the dike direction (in an NNW direction) is well correlated to exposed Strombolian pyroclastic deposits (Fig. 1d) and welded spatter ramparts. This evidence may indicate this area to be the site of the vent system fed by the dike. Interestingly, the linear dike anomaly stops in correspondence with this intense anomaly, constraining the eastern dike-tip position and the location of the vent system. The forward modelling of the anomaly related to the dike was constrained by a field estimate of the total magnetization of the dike samples, which confirmed the high values expected from the intense magnetic anomalies. A profile where the dike is outcropping was used to further constrain the dike model, which resulted to have an inclination of about 80° and with a thickness of about 8.5 m. In the area of the elliptical anomaly, the outcropping volcanic products were modelled with a material having the same magnetization as the dike and a maximum thick-ness of 10–15 m.

6. Conclusions

In recent years the possibility of acquiring magnetic data from UAVs flying at very low altitude is gaining more and more success, with many studies proposing various measurement and flying solutions. One may wonder if these UAV systems really represent a useful innovation, or they are essentially replicating ground measurements results with a lower resolution. We think that the UAV magnetometry plays a primary role especially in difficult ground conditions (e.g., presence of dense vegetation, cultivated areas, swamps, glaciers, lakes, foreshore areas or steep mountain slopes). In this paper we presented a successful application of drone magnetometry that emphasizes its utility in conditions of inaccessibility of the investigated area.

We showed how a drone-borne magnetic dataset, acquired with a careful selection of parameters and after a simple processing, allowed an efficient mapping of an igneous dike intruded in sedimentary rocks, which was exposed by excavation activities in an active quarry, highlighting its direction and its eastern termination. Furthermore, it allowed the identification of a vent area with the presence of volcanic products. Therefore, in the presented case, we think that the drone magnetometry represents a unique tool for a fast and accurate identification of volcanic and sub-volcanic bodies across the entire mountain slope. We expect that in many other instances our strategy to set up the UAV magnetometry could represent an optimal solution for a cheap and fast exploration in fields such as volcanology, mining or structural geology.

CRediT authorship contribution statement

Filippo Accomando: Writing – review & editing, Writing – original draft, Visualization, Validation, Supervision, Software, Resources, Methodology, Investigation, Formal analysis, Data curation, Conceptualization. **Antonello Bonfante:** Resources, Investigation. **Maurizio Buonanno:** Resources, Investigation. **Jacopo Natale:** Writing – original draft, Investigation. **Stefano Vitale:** Writing – original draft, Investigation. **Giovanni Florio:** Writing – review & editing, Writing – original draft, Visualization, Validation, Supervision, Software, Resources, Methodology, Investigation, Formal analysis, Data curation, Conceptualization.

Declaration of Competing Interest

The authors declare the following financial interests/personal relationships which may be considered as potential competing interests:

Filippo Accomando reports administrative support, article publishing charges, equipment, drugs, or supplies, travel, and writing assistance were provided by University of Naples Federico II. Filippo Accomando reports a relationship with University of Naples Federico II that includes: employment and funding grants

Data availability

Data will be made available on request.

Acknowledgments

The aerial surveys were planned and conducted by using the UgCS PRO software. We warmly thank SPH Engineering for the "Educational" conditions under which we could use their product.

The authors are grateful to Colacem SPA for granting the access to the quarry. Dr. Gerardo Iacovone is acknowledged for his cooperation and support. Mario Scardino is acknowledged for his help and support during the surveys.

References

Accomando, F., Vitale, A., Bonfante, A., Buonanno, M., Florio, G., 2021. Performance of two different flight configurations for drone-borne magnetic data. Sensors 21, 5736. https://doi.org/10.3390/s21175736.

Breiner, S., 1973. Applications Manual for Portable Magnetometers. Geometries, 395 Java Drive. Sunnyvale, California, p. 58.

Conticelli, S., Marchionni, S., Rosa, D., Giordano, G., Boari, E., Avanzinelli, R., 2009. Shoshonite and sub-alkaline magmas from an ultrapotassic volcano: Sr–Nd–Pb isotope data on the Roccamonfina volcanic rocks, Roman Magmatic Province, Southern Italy. Contrib. Mineral. Petrol. 157, 41–63.

Cunningham, M., 2018. Aeromagnetic Surveying with Unmanned Aircraft Systems. Master's Thesis, Carleton University, Ottawa, ON, Canada. https://doi.org/10.22215/etd/2016-11270.

De Rita, D., Giordano, G., 1996. Volcanological and structural evolution of Roccamonfina volcano (Italy): origin of the summit caldera. Geol. Soc. Lond. Spec. Publ. 110 (1), 209–224.

De Smet, T.S., Nikulin, A., Romanzo, N., Graber, N., Dietrich, C., Puliaiev, A., 2021. Successful application of drone-based aeromagnetic surveys to locate legacy oil and gas wells in Cattaraugus County, New York. J. Appl. Geophys. 186, 104250 https://doi.org/10.1016/j.jappgeo.2020.104250.

Di Girolamo, P., Melluso, L., Morra, V., 1991. Magmatic activity northeast of Roccamonfina volcano (Southern Italy): petrology, geo-chemistry and relationships with campanian volcanics. Neues Jb. Mineral. Abh. 163, 271–289.

Kaub, L., Keller, G., Bouligand, C., Glen, J.M.G., 2021. Magnetic surveys with Unmanned Aerial Systems: software for assessing and comparing the accuracy of different sensor systems, suspension designs and compensation methods. Geochem. Geophys. Geosyst. 22, e2021GC009745 https://doi.org/10.1029/2021GC009745.

Li, H., Ge, J., Dong, H., Qiu, X., Luo, W., Liu, H., Yuan, Z., Zhu, J., Zhang, H., 2018. Aeromagnetic compensation of Rotor UAV based on least squares. In: Proceedings of the 37 864 th Chinese Control 865 Conference, Wuhan, China, pp. 10248–10253. https://doi.org/10.23919/ChiCC.2018.8483068.

Malehmir, A., Dynesius, L., Paulusson, K., Paulusson, A., Johansson, H., Bastani, M., Wedmark, M., Marsden, P., 2017. The potential of rotary-wing UAV-based magnetic surveys for mineral exploration: A case study from Central Sweden. Lead. Edge 36, 552–557. https://doi.org/10.1190/tle36070552.1.

Mu, Y., Zhang, X., Xie, W., Zheng, Y., 2020. Automatic detection of near-surface targets for unmanned aerial vehicle (UAV) magnetic survey. Remote Sens. 12, 452. https://doi.org/10.3390/rs12030452.

Natale, J., Vitale, S., Giordano, G., Fedele, L., Lucci, F., Vona, A., Prinzi, E.P., Tramparulo, F.D.A., Isaia, R., Ciarcia, S., 2023. The Taverna San Felice dike (NE of Roccamonfina volcano): unravelling magmatic intrusion processes and volcano-tectonics in the Tyrrhenian margin of the southern Apennines. Geochem. Geophys. Geosyst. 24 (8), e2023GC010994.

Nikulin, A., De Smet, T.S., Puliaiev, A., Zhurakhov, V., Fasullo, S., Chen, G., Spiegel, I., Cappuccio, K., 2020. Automated UAS aeromagnetic surveys to detect MBRL unexploded ordnance. J. Conv. Weapons Destruct. 24, 56–62. https://commons.lib.jmu.edu/cisr-journal/vol24/iss1/13.

Parshin, A.V., Morozov, A.V., Blinov, A.N., Kosterev, Budyak, A. E., 2018. Low-altitude geophysical magnetic prospecting based on multirotor UAV as a promising replacement for traditional ground survey. Geo-spatial Inform. Sci. 21, 67–74 doi: 10.1080/10095020.2017.1420508.

Parvar, K., Braun, A., Layton-Matthews, D., Burns, M., 2018. UAV magnetometry for chromite exploration in the Samail ophiolite sequence. Oman. J. Unmanned Veh. Syst. 6, 57–69. https://doi.org/10.1139/juvs-2017-0015.

Phelps, G., Bracken, R., Spritzer, J., White, D., 2022. Achieving sub-nanoTesla precision in multirotor UAV aeromagnetic surveys. J. Appl. Geophys. 206 (1), 104779. https://doi.org/10.1016/j.jappgeo.2022.104779.

Talwani, M., Heirtzler, J.R., 1964. Computation of magnetic anomalies caused by two-dimensional bodies of arbitrary shape. In: Parks, G.A. (Ed.), Computers in The Mineral Industries, Part 1: Stanford Univ. Publ., Geological Sciences, 9, pp. 464–480.

Tuck, L., Samson, C., Polowick, C., Laliberté, J., 2019. Real-time compensation of magnetic data acquired by a single-rotor unmanned aircraft system. Geophys. Prospect. 67, 1637–1651. https://doi.org/10.1111/1365-2478.12800.

Veloski, G.A., Hammack, R.G., Sams III, J.I., Wylie, L.D., Heirendt, K., 2018. Evaluation of the micro-fabricated atomic magnetometer deployed from a small autonomous rotorcraft for locating legacy oil & gas wells. In: Environmental and Engineering Geophysical Society Annual Meeting, Nashville TN, p. 912. https://doi.org/10.4133/sageep.31-002.

Vitale, S., Ciarcia, S., 2018. Tectono-stratigraphic setting of the Campania region (southern Italy). J. Maps 14 (2), 9–21.

Walter, C.A., Braun, A., Fotopoulos, G., 2019a. Impact of 3-D attitude variations of a UAV magnetometry system on magnetic data quality. Geophys. Prospect. 67, 465–479. https://doi.org/10.1111/1365-2478.12727.

Walter, C., Braun, A., Fotopoulos, G., 2019b. Spectral analysis of magnetometer swing in high-resolution UAV-borne aeromagnetic surveys. In: Proceedings of the 2019 IEEE Systems and Technologies for Remote Sensing Applications through Unmanned Aerial Systems (STRATUS), Rochester, NY, USA, pp. 1–4. https://doi.org/10.1109/STRATUS.2019.8713313.

Walter, C., Braun, A., Fotopoulos, G., 2020. High-resolution unmanned aerial vehicle aeromagnetic surveys for mineral exploration targets. Geophys. Prospect. 68, 334–349. https://doi.org/10.1111/1365-2478.12914.

Walter, C., Braun, A., Fotopoulos, G., 2021. Characterizing electromagnetic interference signals for unmanned aerial vehicle geo-physical surveys. Geophysics 86 (6), B321–V488. https://doi.org/10.1190/geo2020-0895.1.

Won, I.J., Bevis, M., 1987. Computing the gravitational and magnetic anomalies due to a polygon: Algorithms and Fortran subroutines. Geophysics 52, 232–238. https://doi.org/10.1190/1.1442298.